Closing report of NKFI-EPR K 115441 grant

The project had administrative, technical and human resource difficulties throughout it course.
For administrative reasons, not revealed to us, the 2-photon microscope that was to be financed from the NAP Infrastructural grant arrived to the Institute only at the end of November 2016 (a year later then due). We started to go on with the plans, but the microscope has been payed for by NAP only with great delays and technical support from the supplier was sporadic for long while. We proceed significantly slower than planned. Finally it turned out, that the 2P calcium imaging technology proved to be far less sensitive, than we expected (in agreement with other colleagues). The biggest problem we saw using 2P calcium imaging was that evidently the calcium signals we record form neurons are present only when a neuron fires bursts, but not single action potentials. The number of detected calcium events are far below the frequency of unit spikes observed form spike sorted materials. We tried to record not from the hippocampus but from the entorhinal cortex and also from primary sensory cortices, since in the neocortex higher activity levels had been reported. We could prepare in vitro enothinal cortical-hippocampal slices where the population activity (measured by electrophysiology) was correlated between the areas, demonstrating working connectivity and physiological-like activity. Unfortunately, here again we could not record signals that we would consider even remotely matching neuronal activity expected from electrophysiological recordings. We also tried to use different viral strains to label inhibitory neuron populations (since their firing frequency is higher than that of pyramidal cells) and measure how are they recruited during epileptiform events (we found that these massive synchronous event lit up during imaging) but could not see signals from them.
Therefore, we considered this approach a complete failure, since we wanted to study the firing pattern of individual pyramidal cells during subsequent sharp-waves. Consequently, we focused our efforts on other projects.
We developed a semi-automatic, quick measurement system to optogenetically drive inputs of different inhibitory neuron classes in different spatial and temporal combinations. We planned to systematically measure the integrative properties of identified neurons. Unfortunately due to chronic problems with able workforce this project has been abandoned.
However we started several collaborations, where we provided our technical expertise in in vitro electrophysiology and optogenetics. These projects resulted four papers in top scientific journals.

Summary

Using anatomical method our collaborators revealed new neurochemically specific subcortical centers and pathways. Then a collaborative work, using in vitro and in vivo electrophysiology combined with optogenetics and behavioral experiments, revealed the functional significance of these elements. We contributed to these results by characterizing neuronal properties and revealing the transmission features of these elements using in vitro electrophysiology. It was shown that: 1) the median raphe region harbors a cell population that activate aversion- and negative prediction–related brain areas and initiate immediate acquisition of episodic memories of the negative experience. 2) nucleus incertus GABAergic neurons (that receive salient environmental information) selectively inhibit a hippocampal interneuron population. The pathway might be important in fine-tuning memory-acquisition, based on the relevance of environmental inputs. 3) two distinct types of basal forebrain cholinergic neurons exist, that differ in their properties and behavioral correlates. 4) cholinergic terminals of basal forebrain origin establish GABAergic synapses in the hippocampus, and their cholinergic vesicles dock at those synapses only. These synapses co- transmit GABA and acetylcholine via different vesicles and evoke composite

postsynaptic potentials. The GABAergic component alone effectively suppresses hippocampal sharp wave-ripples and epileptiform activity.

Summary in Hungarian

Négy új neurokémiailag egyedi kéreg alatti terület illetve pálya leírásában vettünk részt kollaborációk keretében. A sok módszert felvonultató megközelítéshez (anatómia, in vivo vizsgálatok, viselkedés vizsgálat) csoportunk in vitro vizsgálatokkal járult hozzá, melyek a sejtcsoportok tulajdonságait és a jelátvitel sajátosságait tisztázták. A következőket találtuk: 1) A mediális raphe terület egyik sejtcsoportja fontos a negatív tapasztalatokkal kapcsolatos epizódikus memórianyomok kialakításában. 2) a nucleus incertus GABA tartalmú idegsejtjei (melyek a környezet fontos eseményeiről szállítanak infomációt) specifikusan gátolnak egy hippokampális gátlósejt csoportot, ezáltal részt vesznek a fontos eseményekkel kapcsolatos memórianyomok tárolásában. 3) két bazális előagyi cholinerg sejtcsoport azonosítható, melyek a viselkedés eltérő fázisaiban aktiválódnak. 4) bazális előagyi cholinerg végződések GABAt is tartalmaznak a hippokampuszban. A terminálisokban található cholinerg és GABAerg vezikulák külön-külön szabadulnak fel szinaptikus úton, és összetett szinaptikus potenciálokat váltanak ki. A GABAerg komponens egymagában képes gátolni a hippokampéis éles-hullámokat, valamint az epileptikus aktivitást.

Szonyi 2019a, Science

We discovered that the median raphe region (MRR) harbors a vesicular glutamate transporter 2 (vGluT2)– positive cell population that gives rise to the largest ascending output of the MRR. These neurons received extensive inputs from negative sensory experience–related brain centers, whereas their excitatory fibers projected to the LHb, mVTA, and MS/VDB. MRR vGluT2 neurons were selectively activated by aversive but not rewarding stimuli in vivo. Stimulation of MRR vGluT2 neurons induced strong aversion, agitation, and aggression as well as suppressed reward-seeking behavior. Their chronic activation induced depression-related anhedonia. MRR vGluT2 neurons seem to be involved in active responses to negative experience, therefore inducing aggression or avoidance, classical fight-or-flight responses. **Suppression of MRR vGluT2 neurons precisely at the moment of the aversive stimulus presentation strongly disrupted the expression of both contextual and cued fear memories and prevented fear generalization.** MRR vGluT2 neurons could facilitate the learning of negative experience, because their LHb-projecting axons bifurcated and selectively innervated pacemaker MS/VDB PV-positive neurons that projected to the hippocampus. Consequently, in vivo stimulation of MRR vGluT2 neurons instantly evoked memory acquisition–promoting hippocampal theta oscillations in mice.

The **MRR**, thus, harbors a previously unrecognized brainstem center that **serves as a key hub for the acquisition of negative experience.** MRR vGluT2 neurons could **activate the aversion- and negative prediction–related LHb-mVTA axis and** could swiftly **transform the state of the septohippocampal system for immediate acquisition of episodic memories of the negative experience.** Maladaptations in processing negative experience form the basis of several types of mood disorders, which have a huge social and eco- nomic impact on individuals and society. Selective targeting of this neural hub may form the basis of new therapies.

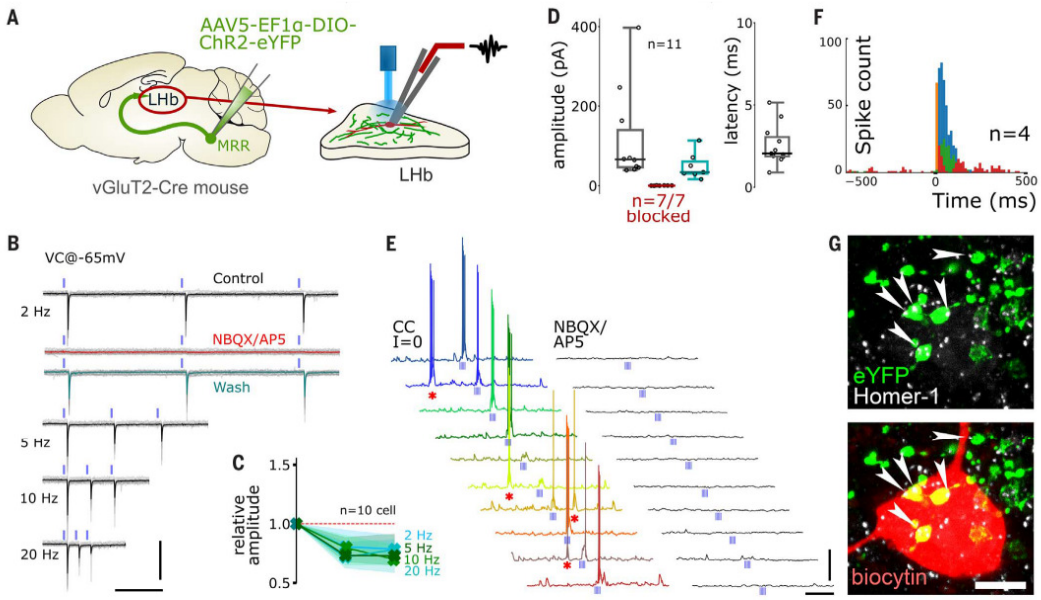

Fig. 3. Fibers of MRR vGluT2 neurons evoke burst firing in LHb neurons. (**A**) AAV2/5-EF1α-DIO-ChR2-eYFP was injected into the MRR of vGluT2-Cre mice (n = 3). Six weeks later, 300-μm-thick horizontal in vitro slices were prepared from the LHb. Neurons in the LHb were whole-cell patch clamped in voltage-clamp mode (see supplementary methods). (**B**) Light stimulations of MRR vGluT2 fibers evoked EPSCs in LHb neurons. The average responses to 2-ms light pulses are shown above individual gray traces. Responses are strong in control conditions (black); they were completely abolished (red trace) by 20-μM NBQX (AMPA/kainite receptor antagonists) and 50-μM AP5 (NMDA antagonist) and partially recovered after washout (teal). Scale bars: 200 ms, 200 pA. (**C**) Cells displayed short-term depression of EPSC amplitudes at all stimulation frequencies (averages from 10 cells). (**D**) EPSC amplitude and latency distributions from all 11 recorded neurons (in gray). Excitatory postsynaptic potentials were sensitive to glutamatergic antagonists in 7 out of 7 tested cells (red) and partially recovered after washout (teal). (**E**) Traces show representative current-clamped (I = 0) LHb neurons displaying spontaneous (asterisks) and light-evoked (pale blue lines, 5 pulses at 20 Hz) bursts. Ten consecutive stimulations are shown. Both spontaneous and light-evoked bursts were abolished by application of NBQX and AP5 (traces on the right). Scale bars: 1 s, 20 mV. (**F**) Peristimulus time histogram shows action potential distributions upon light stimuli (n = 4 cells). (**G**) A representative, recorded LHb cell (biocytin labeling, red) receives Homer-1–positive (white) synaptic contacts (white arrowheads) from eYFP-positive MRR fibers (green). Scale bar: 5 μm.

Szonyi 2019b, Science

We discovered that NI GABAergic neurons (that receive direct inputs from several brain areas processing salient environmental stimuli, including the prefrontal cortex and lateral habenula) selectively inhibit hippocampal SOM interneurons in the stratum oriens both directly and also indirectly through inhibition of excitatory neurons in the medial septum. These salient sensory stimuli (e.g., air puffs, water rewards) rapidly activated hippocampal fibers of NI GABAergic neurons in vivo. Behavioral experiments revealed that optogenetic stimulation of NI GABAergic neurons or their fibers in hippocampus, precisely at the moment of aversive stimuli, prevented the formation of fear memories. In contrast, optogenetic inhibition of NI GABAergic neurons during fear conditioning resulted in the formation of excessively enhanced contextual memories. A role of NI GABAergic neurons may be fine-tuning of the selection of memory-encoding pyramidal cells, on the basis of the relevance and/or modality of environmental inputs. They may also help filter nonrelevant everyday experiences. NI GABAergic neuron dysfunction may also contribute to dementia-like disorders or pathological memory formation in certain types of anxiety or stress disorders.

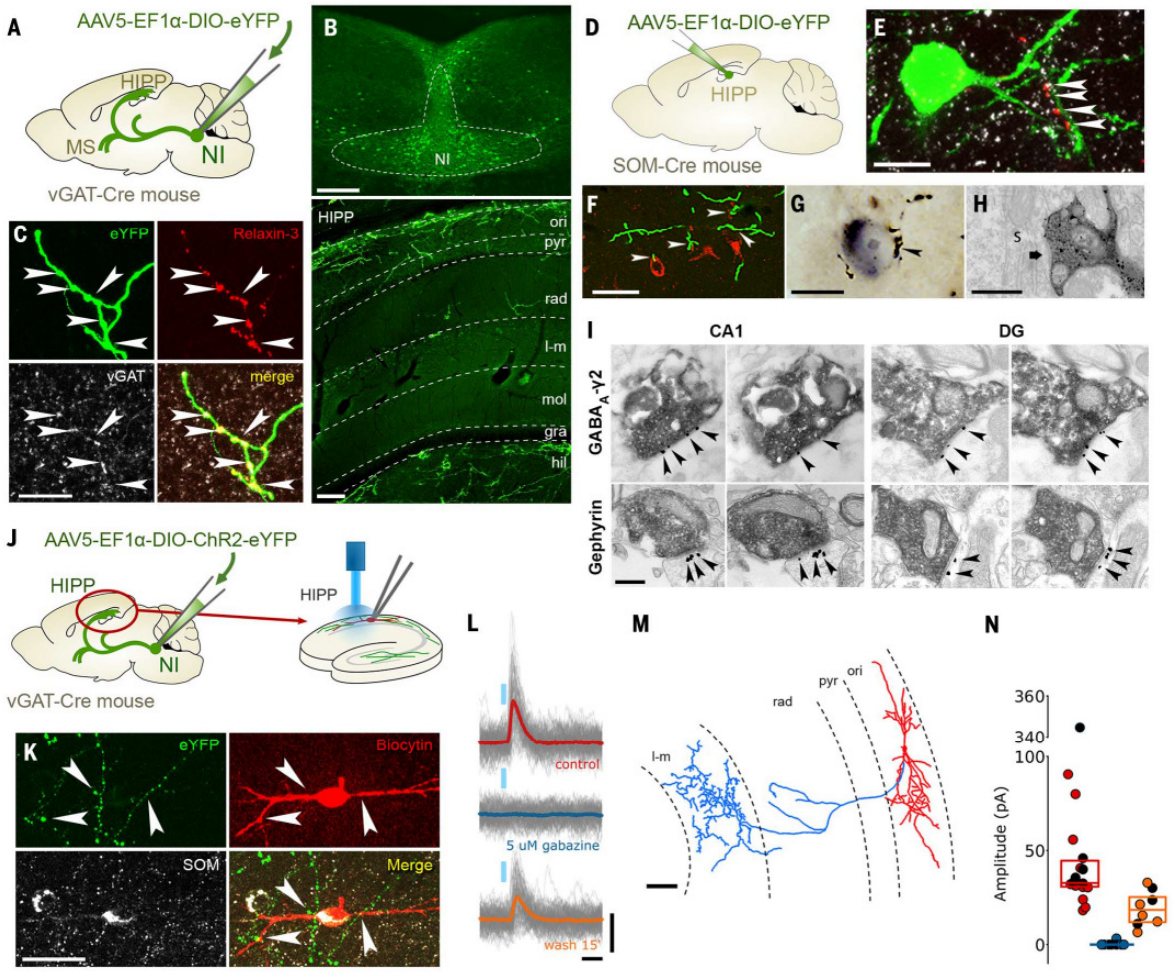

Fig. 1. NI neurons target HIPP SOM-positive neurons with GABAergic synapses. (**A**) AAV2/5-EF1α-DIO-eYFP or AAV2/5-EF1α-DIO-mCherry was injected into the NI of vGAT-Cre mice (n = 7). (**B**) Images illustrate an injection site (upper panel) and the layer-specific distribution pattern of GABAergic NI fibers in the hippocampus (HIPP) stratum oriens and hilus (lower panel) where SOM neurons are known to be abundant. Scale bars: 200 μm. (**C**) NI fibers (green) in the HIPP are immunopositive for relaxin-3 (red) and vGAT (white). Scale bar: 10 μm. (See supplementary text for Fig. 1.) (**D**) AAV2/5-EF1α-DIO-eYFP was injected into the bilateral hippocampus of SOM-Cre mice (n = 2). (**E**) Relaxin-3–positive NI fibers (red) establish synaptic contacts, marked by gephyrin (white), on SOM-positive interneurons (green) in the HIPP. Scale bar: 10 μm. (See supplementary text for Fig. 1.) (**F**) eYFP-positive NI GABAergic fibers (green) in the HIPP establishing putative contacts (white arrowheads) with SOM-positive interneurons (red). Scale bar: 20 μm. (**G**) NI GABAergic fibers (labeled with brown silver-gold-intensified-DAB precipitate) establish synaptic contact with a SOM-positive interneuron (labeled with black DAB-Ni precipitate) in the stratum oriens of dorsal CA1. Black arrowhead indicates the NI nerve terminal shown in (G). Scale bar: 10 μm. (**H**) The same terminal marked in (F) establishing a symmetrical synaptic contact (black arrow) on the soma (s) of the SOM-positive interneuron. Scale bar: 600 nm. (**I**) Electron microscopy (EM) images of serial sections of AAV-eYFP–positive NI terminals (immunoperoxidase labeling, black DAB precipitate) that establish symmetrical synaptic contacts in the CA1 stratum oriens or in the hilus (DG), containing the GABA$_A$ receptor γ2 subunit (upper row) and the scaffolding protein gephyrin (lower row). The immunogold particles labeling the postsynaptic proteins are marked by black arrowheads. Scale bar: 300 nm. (See supplementary text for Fig. 1). (**J**) For in vitro recordings, AAV2/5-EF1α-DIO-ChR2-eYFP was injected into the NI of vGAT-Cre mice (n = 9). After 6 weeks, 300-μm-thick horizontal slices were prepared from the HIPP and transferred into a dual superfusion chamber. Interneurons located in the stratum oriens were whole-cell patch-clamped in voltage-clamp mode, and inhibitory postsynaptic currents (IPSCs) evoked by the optogenetic stimulation of NI GABAergic fibers were measured. (See supplementary materials and methods and supplementary text for Fig. 1.) (**K**) A representative recorded cell (biocytin labeling, red) identified as a SOM-positive interneuron (white). Note that the eYFP-positive NI GABAergic fibers (green) with putative contacts target this neuron (arrowheads). Scale bar: 30 μm. (**L**) Optogenetically evoked GABAergic IPSCs of interneuron in (K). One hundred consecutive traces evoked by 2-ms light pulses are overlaid with gray in each condition. Responses are strong in controls (average in red) but were completely abolished by 5 μM gabazine (average in blue) and partially recovered after 15 min of washout (average in orange). Scale bars: 10 ms, 40 pA. (**M**) Morphological reconstruction of the OLM cell shown in (K). Scale bar: 50 μm. (**N**) Postsynaptic current amplitude distribution from all 18 recorded neurons. Identified O-LM cells are filled black dots. (See supplementary text for Fig. 1.)

Laszlovszky 2020, Nature Neuroscience

We recorded Basal forebrain cholinergic neurons (BFCNs) in vivo, to examine their behavioral functions, and in vitro, to study their intrinsic properties. We identified two distinct types of BFCNs that differ in their firing modes, synchronization properties and behavioral correlates. Bursting cholinergic neurons (Burst-BFCNs) fired synchronously, phase-locked to cortical theta activity and fired precisely timed bursts after reward and punishment. Regular-firing cholinergic neurons (Reg-BFCNs) were found predominantly in the posterior basal forebrain, dis-played strong theta rhythmicity and responded with precise single spikes after behavioral outcomes. Synchronization of Burst-BFCNs to the cortex predicted the timing of behavioral responses, whereas evoked cortical coupling of Reg-BFCNs predicted correct detections. We propose that differential recruitment of two basal forebrain cholinergic neuron types generates behavior-specific cortical activation.

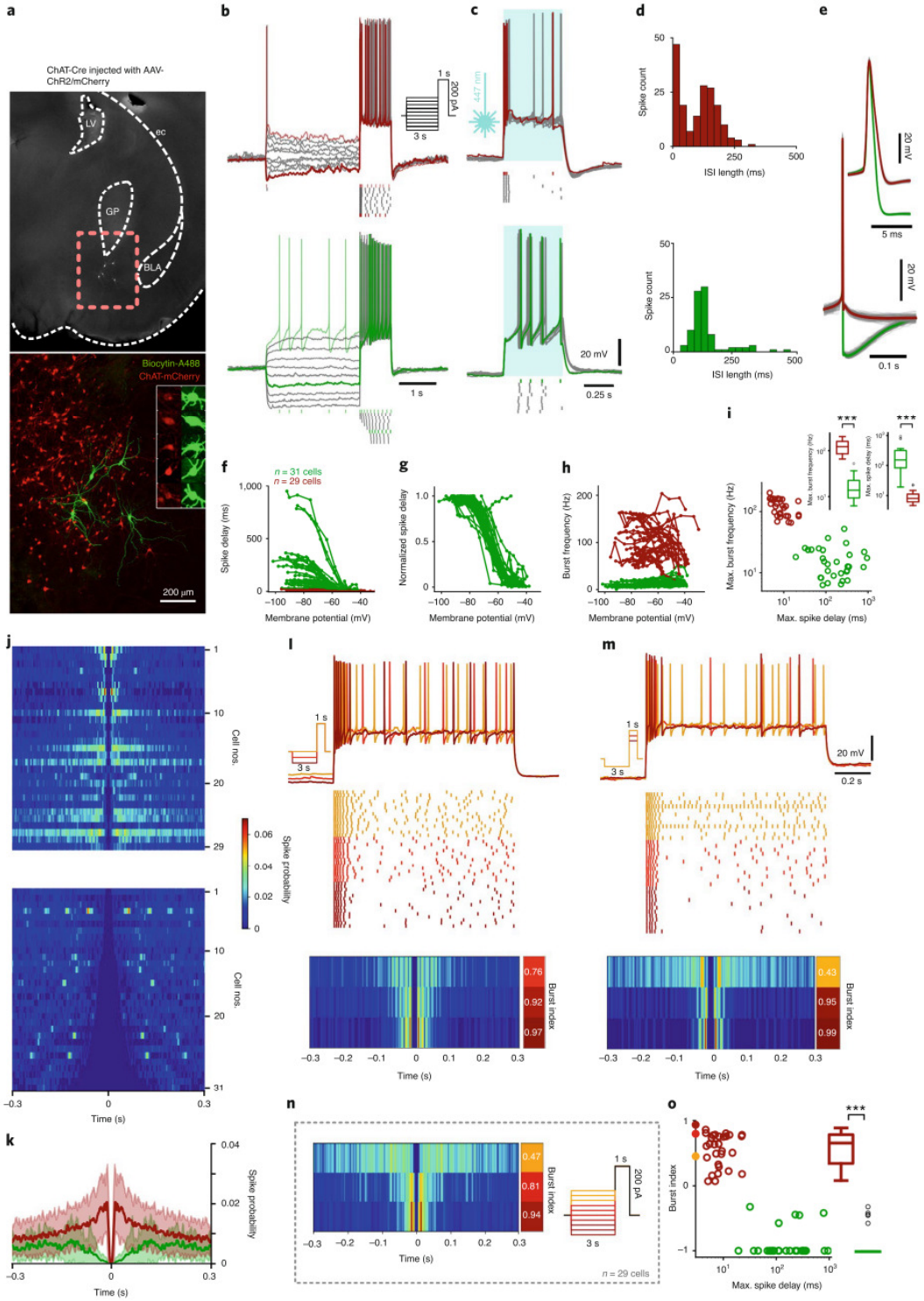
a
ChAT-Cre injected with AAV-ChR2/mCherry
LV
ec
GP
BLA
Biocytin-A488
ChAT-mCherry
200 μm
b
1 s
200 pA
3 s
1 s
c
447 nm
20 mV
0.25 s
d
Spike count
ISI length (ms)
e
20 mV
5 ms
0.1 s
f
n = 31 cells
n = 29 cells
Spike delay (ms)
Membrane potential (mV)
g
Normalized spike delay
Membrane potential (mV)
h
Burst frequency (Hz)
Membrane potential (mV)
i
Max. burst frequency (Hz)
Max. spike delay (ms)
j
Cell nos.
Spike probability
Time (s)
k
Spike probability
Time (s)
l
1 s
3 s
Burst index
Time (s)
m
1 s
3 s
20 mV
0.2 s
Burst index
Time (s)
n
Burst index
Time (s)
1 s
200 pA
3 s
n = 29 cells
o
Burst index
Max. spike delay (ms)

Fig. 2 | In vitro recordings confirmed two types of central cholinergic neurons. a, Representative confocal image of recorded and biocytin-filled cholinergic cells expressing ChR2 in the nucleus basalis of the BF. **b**, Top: firing pattern of an early-firing cell, showing short spike delay and high-frequency spike clusters on positive current injections. Bottom: firing pattern of a representative late-firing cholinergic cell, showing low maximal firing rate and prominent spike delay when driven from hyperpolarized membrane states. **c**, The same cells show similar responses on photostimulation (0.5 s). **d**, ISI histograms of the same cells show bimodal (early-firing) or unimodal (late-firing) distributions. **e**, Average AP shape from an example early-firing (red) and late-firing (green) cholinergic cell (100 APs per cell in gray, average in color). **f**, Spike delay depended on the membrane potential ($n = 31$ for late-firing and $n = 29$ for early-firing cholinergic cells). **g**, Normalized spike delay showed stereotypical behavior in late-firing cholinergic neurons ($n = 31$). **h**, Maximal burst frequency as a function of the membrane potential ($n = 31$ late-firing and $n = 29$ early-firing cholinergic cells). **i**, Maximal burst frequency plotted against maximal spike delay in all recorded cells ($n = 31$ late-firing and $n = 29$ early-firing cholinergic cells). $^{***}P < 0.001$; maximal spike delay, $P = 2.08 \times 10^{-11}$; maximal burst frequency, $P = 1.54 \times 10^{-11}$; two-sided Mann–Whitney *U*-test. Box-and-whisker plots show median, interquartile range, nonoutlier range and outliers. **j**, Spike auto-correlograms during somatic current injection protocols for all cells (top: $n = 29$ early-firing cholinergic cells; bottom: $n = 31$ late-firing cholinergic cells). **k**, Average auto-correlograms of early-firing (red, $n = 29$) and late-firing (green, $n = 31$) cholinergic cells (solid lines, mean; shading, s.e.m.). **l**, Firing pattern of an early-firing cell in response to three current injection protocols, with different current magnitude applied before the depolarization step. The protocol was designed to model the internal state (membrane potential) dependence of the spiking pattern in response to a uniform input. Raster plot represents 20 trials with each protocol (deeper red, more hyperpolarized states). Bottom: corresponding auto-correlograms and burst indices. **m**, Firing pattern of the same cell in response to current injection protocols with different depolarization step magnitudes. The protocol was designed to mimic input strength dependence of the spiking pattern. Raster plot shows 20 trials for each protocol, with a deeper red corresponding to smaller injected currents. **n**, Average ACGs and corresponding burst indices of early-firing cells ($n = 29$) driven from depolarized (top) and hyperpolarized (bottom) states. Three groups were formed from all early-firing cells based on the 3-s-long prepolarization magnitude (right inset). **o**, Burst index plotted against maximal spike delay ($n = 31$ late-firing and $n = 29$ early-firing cholinergic cells). Dots overlaid on the *y* axis correspond to the burst indices presented in **n**. Burst indices: $^{***}P < 0.001$, $P = 2.11 \times 10^{-12}$; two-sided Mann–Whitney *U*-test. Box-and-whisker plots show median, interquartile range, nonoutlier range and outliers.

Takacs 2018, Nature Communications

We found that cholinergic terminals of basal forebrain origin establish GABAergic synapses in the hippocampus, and their cholinergic vesicles dock at those synapses only. We demonstrate that these synapses do not co-release but co- transmit GABA and acetylcholine via different vesicles, whose release is triggered by distinct calcium channels. This co-transmission evokes composite postsynaptic potentials, which are mutually cross-regulated by presynaptic autoreceptors. The GABAergic component alone effectively suppresses hippocampal sharp wave-ripples and epileptiform activity. Therefore, the differentially regulated GABAergic and cholinergic co- transmission suggests a hitherto unrecognised level of control over cortical states. This novel model of hippocampal cholinergic neurotransmission may lead to alternative pharmacotherapies after cholinergic deinnervation seen in neurodegenerative disorders.

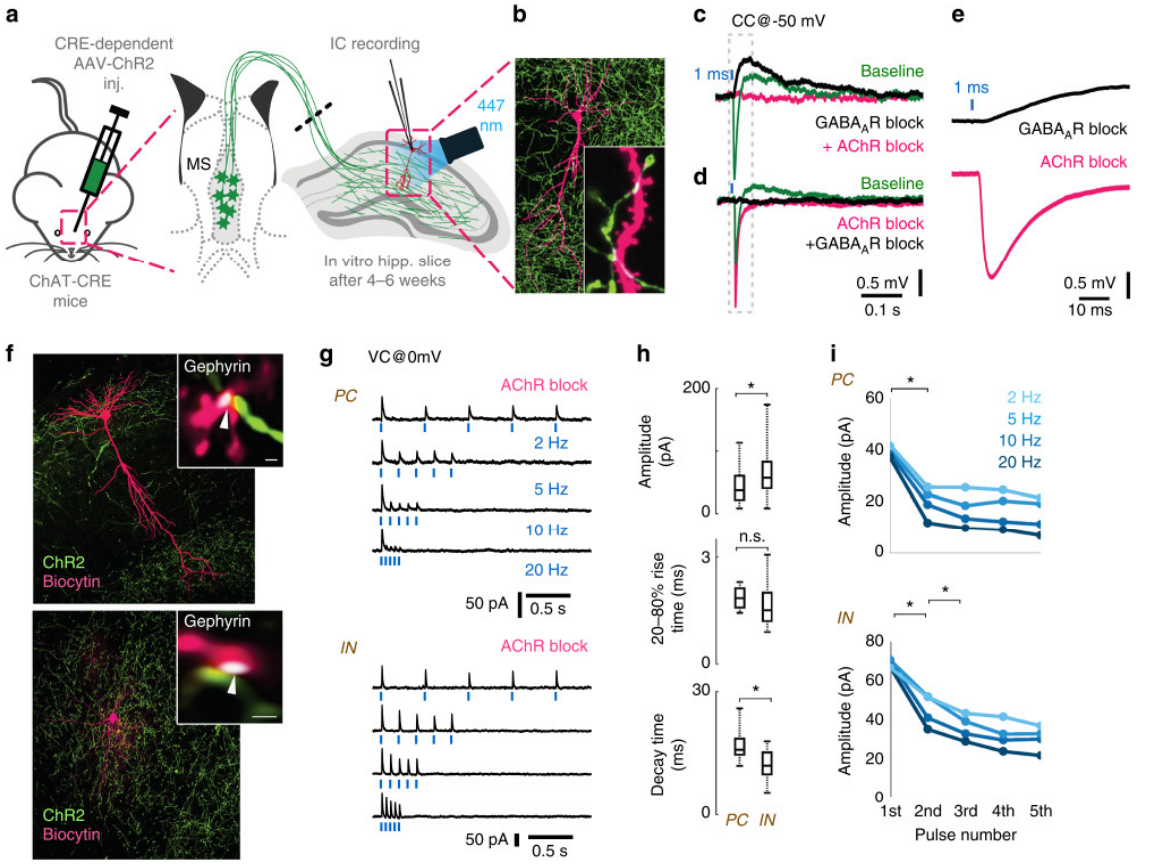

Fig. 3 Optogenetic stimulation of cholinergic fibres elicits composite GABAergic and cholinergic postsynaptic responses. **a** Medial septum (MS) of ChAT-Cre mice were injected with Cre-dependent AAV containing Channelrhodopsin-2 (ChR2). Using whole-cell patch-clamp in horizontal hippocampal slices, we recorded voltage or current response from hippocampal neurons upon optical excitation of septo-hippocampal cholinergic fibres. NMDA and AMPA receptors were blocked with AP5 (50 μM) and NBQX (20 μM) in all experiments presented in Figs. 3 and 5. **b** Representative post-hoc visualised CA1 pyramidal cell (magenta) and the surrounding cholinergic fibres (green) with putative contacts (inset, white arrowheads). **c** Blue light pulses elicited a composite membrane potential response from str. lacunosum-moleculare inhibitory neurons (green, average of 50 stimulations). Inhibition of $GABA_A$Rs (10 μM gabazine) abolishes the hyperpolarising component (nine from nine tested cells), resulting in a putative cholinergic excitatory potential (black). Inhibition of all AChRs (1 μM MLA, 1 μM DHβE, 10 μM atropine, four from four tested cells) blocks the remaining depolarising response (magenta). **d** Conversely, first blocking the AChRs, resulted in a putative GABAergic IPSP (magenta), which was blocked by $GABA_A$Rs inhibitor gabazine (black). The increase of IPSP amplitude for AChR block is addressed in Fig. 5. **e** Magnified cholinergic EPSP (black) from **c**, and GABAergic IPSP from **d** (magenta) demonstrate their short latency (see also Supplementary Figure 3). **f** A representative recorded pyramidal cell (PC, top) and an inhibitory neuron (IN, bottom) post-hoc visualised in magenta and ChR2 positive cholinergic axons in green. Insets: Immunostaining for gephyrin (white) identify their putative synapses (white arrows). **g** We blocked both nicotinic and muscarinic AChRs (1 μM MLA, 1 μM DHβE, 10 μM atropine) and recorded inhibitory postsynaptic currents (IPSC) evoked by cholinergic fibre illumination. Traces show IPSC response of a PC and an IN to five light pulses (1 ms) at increasing stimulation frequencies (2, 5, 10, 20 Hz, cells were recorded in VC@0 mV). **h** Amplitude and decay time of unitary GABAergic IPSCs from pyramidal cells ($n = 5$) and inhibitory neurons ($n = 16$) were statistically different ($p < 0.05$), while their rise time was not different (median values, interquartile ranges and min/max values, see Supplementary Note 8). **i** Averages of IPSC amplitudes for the five pulses presented on **g** shows strong short-term depression (STD) of GABAergic transmission evoked by stimulating cholinergic fibres (for details see Supplementary Note 8 and Supplementary Figure 3)